Acceleration of electrically charged particles
along an escape corridor from an accretion disk:
Onset of chaos near a magnetised black hole

Vladimír Karas & Ondřej Kopáček *(Astronomical Institute, Czech Academy of Sciences, Prague)*

Devaky Kunneriath *(National Radio Astronomy Observatory, Charlottesville, VA)*

Astronomical Institute
of the Czech Academy of Sciences

We examine a mechanism of destabilisation of equatorial orbits of electrically charged particles and dust grains. Near a magnetised black hole, initially bound charges can be accelerated along trajectories emerging from an accretion disk that eventually may escape in the vertical direction. A fraction of these trajectories exhibit chaotic behaviour; even for large-scale, ordered magnetic fields it appears that the chaotic dynamics controls the outflow. We employ Recurrence Plots to characterize the onset of chaos in the medium. The role of black hole spin and the magnetic field strength are discussed, and the maximal escape velocity is computed (based on a recent paper, Kopáček & Karas 2018, ApJ, 853, id. 53, 2018; arXiv:1801.01576).

Introduction

We explore the mechanism of particle acceleration from an inner accretion disc near a black hole into a compact corona, and further out. To this end we assume the case of an organised magnetic field near a supermassive black hole [1, 2]. The set-up of our model is relevant also from another angle: exploring the dynamical properties of the particle motion near magnetised black hole or a compact star [3]. We employ the method of Recurrence Plots and we compare them with Poincare surfaces of section. We describe the Recurrence Plots in terms of the Recurrence Quantification Analysis, which allows us to identify the transition between different dynamical regimes of regular vs. chaotic motion [5]. This new technique is able to detect the chaos onset very efficiently, and to provide its quantitative measure. We find that the role of the black-hole spin in setting chaos is more complicated than initially thought. We discuss appropriate ways of characterizing regularity and the degree of chaotic motion in GR [11].

Our picture includes generic building blocks of astrophysically realistic galactic nuclei. On sub-parsec scales, a supermassive black hole is surrounded by a dense Nuclear Star-Cluster and its gaseous environment [12]. The three components are in mutual interaction, which leads to interesting effects. We focus our attention to the possibility of acceleration of electrically charged particles in potential valleys and near magnetic null points that can develop, under suitable circumstances, within the interacting magnetosphere of the black hole – star system. Previously, we investigated the motion of the charged test particles around a Schwarzschild body with the rotating dipole magnetic field frozen in rigidly co-rotating magnetospheric plasma. This field allows motion in the off-equatorial lobes for suitably selected values of parameters of the system [4].

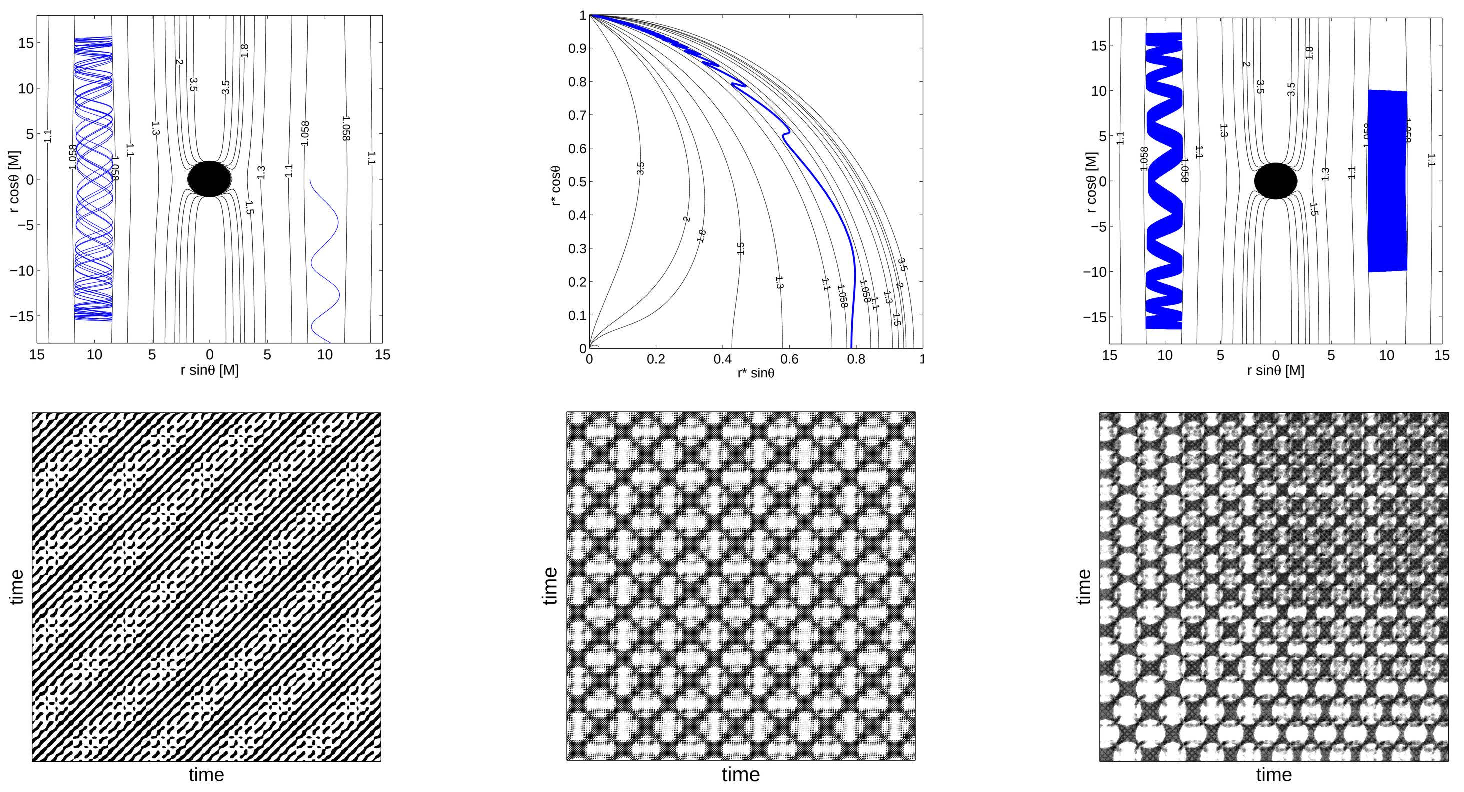

Fig. 1: A sketch of the model set-up. An exemplary trajectory ($\tilde{E} = 1.058$, $\tilde{L} = 5M$) has been launched from the black hole equatorial plane $\theta(0) = \frac{\pi}{2}$ with $u^r(0) = 0$. An external magnetic test field has been imposed in the vertical direction. Parameters of the background are $a = 0.5M$, $\tilde{q}B_0 = 0.1M^{-1}$, $\tilde{q}\tilde{Q} = 1.03$. In the upper left panel we observe that setting $r(0) = 8.4M$ results in oscillations around the equatorial plane while launching it at $r(0) = 8.7M$ makes it escape. In the upper middle panel we examine the trajectory of the escaping particle in terms of the rescaled radial coordinate $r^* \equiv \frac{r-r_+}{r}$. In the case of oscillating trajectories two distinct modes of motion are observed (upper right panel). The first particle ($r(0) = 11.5M$) shows a complex "ribbon-like" trajectory; the other one ($r(0) = 8.4M$) fills uniformly the given portion of the potential valley. The Recurrence Plots are also shown (bottom row). We observe a highly ordered regular pattern for the particle with $r(0) = 8.4M$ (bottom left panel), a more complicated diagonal pattern of the ribbon–like trajectory (launched at $r(0) = 11.5M$, middle panel), and a disrupted diagonal pattern of the transitional trajectory ($r(0) = 11.4M$, bottom right panel).

Equations of motion and the effective potential: an axially symmetric case

The motion of the test matter (particles of charge q and mass m) is given by "super-Hamiltonian"

$$\mathcal{H} = \tfrac{1}{2}g^{\mu\nu}(\pi_\mu - qA_\mu)(\pi_\nu - qA_\nu), \quad \mathrm{d}x^\mu/\mathrm{d}\lambda = \partial\mathcal{H}/\partial\pi_\mu, \quad d\pi_\mu/d\lambda = -\partial\mathcal{H}/\partial x^\mu, \tag{1}$$

where π_μ is the generalized (canonical) momentum and A_μ denotes the vector potential related to the electro-magnetic field tensor as $F_{\mu\nu} = A_{\nu,\mu} - A_{\mu,\nu}$, $\lambda = \tau/m$ is the affine parameter and τ the proper time.

The second Hamilton's equation ensures that the momenta $\pi_t = p_t + qA_t \equiv -E$, $\pi_\phi = p_\phi + qA_\phi \equiv L$ represent constants of motion, reflecting stationarity and axial symmetry of the considered background.

Numerical integration of the Hamilton's equations eq. (1) is carried out using the multistep Adams-Bashforth-Moulton solver of variable order. In several cases when higher accuracy is demanded we employ 7-8th order Dormand-Prince method. Initial values of non-constant components of the canonical momentum $\pi_r(0)$ and $\pi_\theta(0)$ are obtained from $u^r(0)$ (which we set) and $u^\theta(0)$ which is calculated from the normalization condition $g^{\mu\nu}u_\mu u_\nu = -1$ where we always choose the non-negative root as a value of $u^\theta(0)$.

Two-dimensional (i.e. related to the motion in two coordinates, r and θ) effective potential ca be expressed as follows:

$$V_{\mathrm{eff}}(r,\theta;\ \tilde{q}\mathcal{M},\ \tilde{L},\ \Omega) = -\frac{3\tilde{q}\mathcal{M}\mathcal{R}\Omega\sin^2\theta}{8M^3} + \left(1-\frac{2M}{r}\right)^{\frac{1}{2}}\left[1+\left(\frac{\tilde{L}}{r\sin\theta}+\frac{3\tilde{q}\mathcal{M}\mathcal{R}\sin\theta}{8M^3 r}\right)^2\right]^{\frac{1}{2}}, \tag{2}$$

where we introduce specific quantities $\tilde{L} \equiv L/m$ and $\tilde{q} \equiv q/m$. $\mathcal{M}$ is the magnetic dipole moment, Ω is the angular velocity of the rigidly co-rotating magnetosphere, and $\mathcal{R}$ is defined by eq. (5).

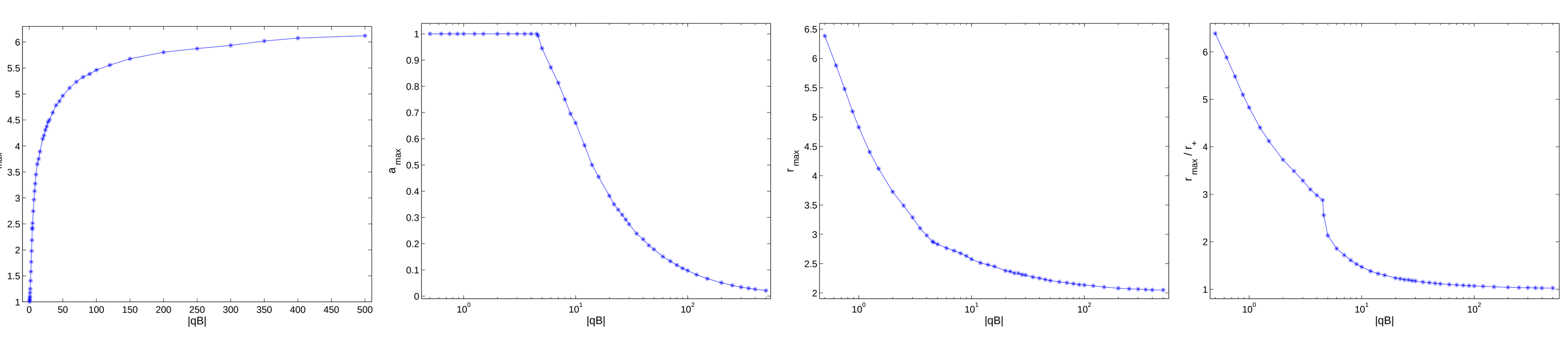

Fig. 2: From left to right: a) Final Lorentz factor $\gamma_{\max}$ of the maximally accelerated escaping orbit is shown as a function of the magnetization parameter $|qB|$. Higher values of spin generally lead to more accelerated escaping orbits. b) The value of spin $a_{\max}$ corresponding to the maximally accelerated escaping orbit. Above the value $|qB| \approx 4.5$ the escape of particles is only permitted for $a < 1$ and the actual value of $a_{\max}$ (which corresponds to the highest allowed value) falls steeply as $|qB|$ increases. c) The initial radius $r_{\max}$ of the maximally accelerated escaping orbit. d) The ratio $r_{\max}/r_+$ of the initial radius and the location of the outer horizon corresponding to the maximally accelerated escaping orbit. Increasing the magnitude of the magnetization parameter shifts the whole escape zone closer to the horizon.

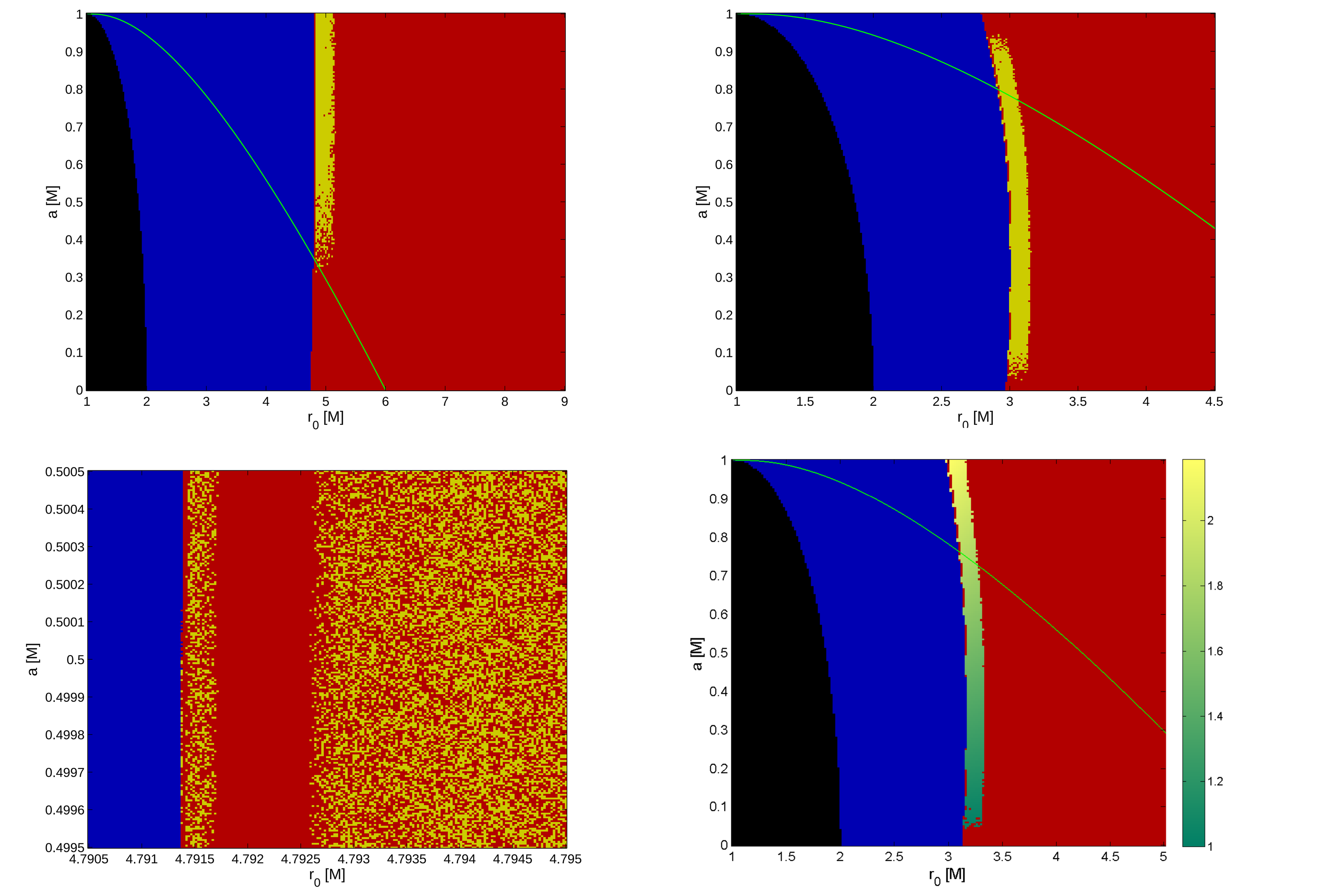

Fig. 3: Characterizing different families of particles that follow free (stable) circular trajectories (free-falling under ISCO) in the Kerr spacetime. Magnetization and the particle charge are set to $qB = -1$ (top left panel) and -5 (top right panel), respectively. Depending on the parameter values and the initial radius, a particle falls directly onto the horizon (blue), remains oscillating in the equatorial plane (red), or it escapes to infinity along the symmetry axis (yellow). Black color denotes the outer horizon of the black hole. The position of ISCO is indicated by the green line. Analysis of the asymptotic behavior shows that only particles with $qB < 0$ can reach infinity. Even particles freely falling from the ISCO may still escape the attraction of the center. Further, we also resolve the fine fractal structure of the escape zone in the case $qB = -1$ (bottom left panel), and the color-coded graph of the terminal Lorentz factor with $qB = -4$ (bottom right panel; the color bar denotes the γ factor of the escaping particles).

Magnetized black hole: a non-rotating case

We describe the gravitational field outside a compact star by the Schwarzschild metric in a non-rotating case,

$$\mathrm{d}s^2 = -\left(1-\frac{2M}{r}\right)\mathrm{d}t^2 + \left(1-\frac{2M}{r}\right)^{-1}\mathrm{d}r^2 + r^2(\mathrm{d}\theta^2 + \sin^2\theta\,\mathrm{d}\phi^2). \tag{3}$$

The associated magnetic field is modeled as a dipole rotating at angular velocity Ω [3]:

$$A_t = -\Omega A_\phi = \frac{3\mathcal{M}\Omega\mathcal{R}\sin^2\theta}{8M^3}, \quad A_\phi = -\frac{3\mathcal{M}\mathcal{R}\sin^2\theta}{8M^3}, \tag{4}$$

where $\mathcal{M}$ is the dipole moment and

$$\mathcal{R} = 2M^2 + 2Mr + r^2\log\left(1-\frac{2M}{r}\right). \tag{5}$$

Alternatively, in order to describe the imposed magnetic field we assume a homogeneous (Wald's) solution. Kerr metric is employed to describe the case of black hole with rotation.

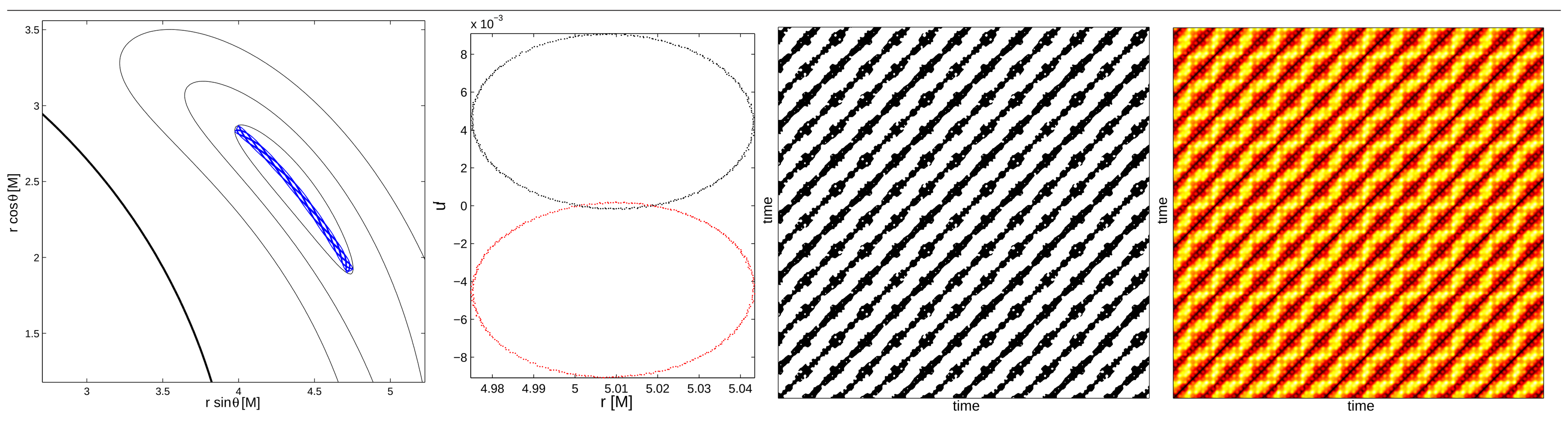

Fig. 4: We trace the trajectory of the test particle ($\tilde{q}\mathcal{M} = -5.71576\ M^2$, $\tilde{L} = 0.87643\ M$) launched above the off-equatorial potential minimum of type Ia ($r(0) = 5\ M$, $\theta(0) = \pi/3$ and $u^r = 0$) at the energy level of $\tilde{E} = 0.848$. The trajectory exhibits standard regular behaviour in the Poincaré surface of section ($\theta_{\mathrm{section}} = \theta(0) = \pi/3$). We distinguish $u^\theta \geq 0$ (black point) from $u^\theta < 0$ (red point) in the surface of section. In the third panel we observe the recurrence plot, which is dominated by diagonal patterns as a general signature of regular motion. In the last panel from left the distance to the recurrence point is color-coded.

Recurrence plots and recurrence quantification analysis

Recurrence plots (RPs) as a tool to visualize recurrences of the trajectory in the phase space were introduced by Eckmann et al in 1987 [7]. RP method is based on examination of the binary values that are constructed from the trajectory $\vec{x}(t)$. Construction of RPs is simple and straightforward regardless of the dimension of the phase space which is a major advantage of this approach. Binary values of the recurrence matrix $\mathbf{R}_{ij}$ may be formally expressed as follows:

$$\mathbf{R}_{ij}(\varepsilon) = \Theta(\varepsilon - ||\vec{x}(i) - \vec{x}(j)||), \quad i,j = 1,...,N \tag{6}$$

where ε is a predefined threshold parameter, Θ represents Heaviside step function and N specifies the sampling frequency which is applied to the examined time period of the trajectory $\vec{x}(t)$. Selection of the norm $||.||$ which should be used to detect recurrences in the phase space is not straightforward. Although simple norms like L^2 (Euclidean norm) are usually applied directly, we want to reflect the curvature of the spacetime as much as possible. Thus we measure distances in the ZAMO's hypersurfaces of simultaneity following the standard $3+1$ splitting procedure [8].

Binary valued matrix $\mathbf{R}_{ij}$ represents the RP which we get by assigning a black dot where $\mathbf{R}_{ij} = 1$ and leaving a white dot where $R_{ij} = 0$. Both axis represent time period over which the data set (phase space vector) is examined. RP is thus symmetric and the main diagonal is always occupied by the line of identity (LOI). Recurrence quantification analysis (RQA) [5] takes number of statistic measures of recurrence matrix $\mathbf{R}_{ij}$. We adapted CRP ToolBox for Matlab (http://www.agnld.uni-potsdam.de/˜marwan/toolbox/) to perform RQA computation.

Acknowledgments. This work has been supported by the project of the Czech Science Foundation (ref. 17-16287S) "Oscillations and Coherent Features in Accretion Disks around Compact Objects and Their Observational Signatures".

Conclusions

From our analysis we conclude that the motion of charged test particles in the off-equatorial lobes allowed by the test field of the rotating magnetic dipole on the Schwarzschild background is largely regular. Once the specific energy $\tilde{E}$ is increased (i.e. the off-equatorial lobe is extended) close to the level where both lobes merge with each other, the chaos may appear. For even higher energies, the lobes merge and chaotic motion becomes typical but, quite surprisingly, also very stable orbits exist under these circumstances.

Acceleration of the escaping particles changes with the spin as well as with the radius of original orbit. Maximally accelerated escaping orbit for given value of qB corresponds to the highest allowed spin and the lowest radius of original orbit, i.e., is located in the upper left corner of the escape zone in presented plots. The value of final Lorentz factor seems to saturate at $\gamma_{\max} \approx 6$. Higher values of spin generally lead to more accelerated escaping orbits.

We demonstrated that the recurrence plots and recurrence quantification analysis are simple, yet powerful tools which allow one not only to decide whether the dynamic regime of the motion is regular or chaotic but also to locate (in terms of some control parameter – energy $\tilde{E}$ in our case) the transition between these regimes with very good precision. Major drawback (cost we pay for its simplicity) of RPs and RQA is the lack of invariance (dependence on the threshold ε, $l_{\min}$, choice of the norm etc.). We conclude that RPs themselves may act as an alternative tool to Poincaré surfaces of section and RQA measures are able to detect the transitions between the dynamic regimes.

References

[1] Kopáček, O., Karas, V., Kovář, J., Stuchlík, Z.: Transition from regular to chaotic circulation in magnetized coronae near compact objects, ***Astrophysical Journal***, 722, 1240-1259, 2010

[2] **Kopáček, O., Karas: Near-horizon structure of escape zones of electrically charged particles around weakly magnetized rotating black hole, *Astrophysical Journal*, 853, id. 53, 2018**

[3] Sengupta, S.: General relativistic effects on the induced electric field exterior to pulsars, *Astrophysical Journal*, 449, 224, 1995

[4] Kovář, J., Kopáček, O., Karas, V., Stuchlík, Z.: Off-equatorial orbits in strong gravitational fields near compact objects II, *Classical and Quantum Gravity*, 27, 135006, 2010

[5] Marwan, N., Carmen Romano, M., Thiel, M., Kurths, J.: Recurrence plots for the analysis of complex systems, *Physics Reports*, 438, 237-329, 2007

[6] Misner C. W., Thorne K. S. and Wheeler J.A.: Gravitation, Freeman, San Francisco, 1973

[7] Eckmann, J.-P., Oliffson Kamphorst, S., Ruelle, D.: Recurrence plots of dynamical systems, *Europhysics Letters*, 5, 973-977, 1987

[8] Thorne, K. S., MacDonald, D.: Electrodynamics in Curved Spacetime – 3+1 Formulation, *Monthly Notices of the Royal Astronomical Society*, 198, 339, 1982

[9] Thiel, M., Romano, M .C., Kurth J.: How much information is contained in a recurrence plot?, *Physics Letters A*,330, 343-349, 2004

[10] Kopáček, O., Karas, V., Kovář, J., Stuchlík, Z.: Application of a symplectic integrator in a non-integrable relativistic system, *Proceedings of RAGtime 10-13: Workshops on black holes and neutron stars* (Opava, Czech Republic), p. 123, 2016 (arXiv:1601.01262)

[11] Kopáček, O., Karas, V., Kunneriath, D., Hamerský, J.: Oblique magnetic fields and the role of frame dragging near rotating black hole, *Acta Polytechnica*, 54, 398, 2014 (arXiv:1408.2452)

[12] Schödel R., Feldmeier A., Kunneriath D., Stolovy S., Neumayer N., Amaro-Seoane P., & Nishiyama S.: Surface brightness profile of the Milky Way's nuclear star cluster, *Astronomy & Astrophysics*, 566, id. A47

E-mail: vladimir.karas@cuni.cz